EXPERIMENTAL AND NUMERICAL APPROACH TO VALIDATE PRESSURE LOSS PREDICTABILITY OF A COMMERCIAL CODE

Tsutomu Ikeno and Shumpei Kakinoki

Nuclear fuel Industries, Ltd.

Abstract

Experimental and numerical works to validate a commercial CFD code for predicting the pressure loss of a PWR grid spacer were presented. The experimental data was obtained for full size spacer mock-ups with different inclination of mixing-vanes. The pressure loss in the complex configuration of spacers arises from a several hydrodynamic effects included in the flow. Only the experimental result therefore was not enough to provide detailed data for validating the turbulence model used in the CFD code. To this end this study used a large eddy simulation (LES) to look at the hydrodynamic effects. The result of the LES indicated that the flow field around the spacer included a large-scale unsteadiness and an undeveloped turbulent flow. Turbulence models based on a developed turbulent flow were theoretically inapplicable to these flows. The commercial code with the standard high Reynolds number k-ε model with the law of the wall however successfully reproduced the trend of the measurement. This suggests that a large-scale unsteadiness and an undeveloped turbulent flow are not dominant for the pressure loss. It is noted that commercial codes should be applied to the flows where dominant physics is clarified.

1. INTRODUCTION

The pressure loss is important for designing the nuclear fuel assembly. The loss coefficient for the spacer is an input parameter for subchannel analysis, and the value has been measured in mock-up experiments. Constructing mock-ups for all the candidates costs much at the planning phase. Computational fluid dynamics (CFD) is expected to screen the candidates and to save the cost.

Thus validating the CFD code for predicting pressure loss of the spacer becomes important. The pressure loss is fundamentally a macroscopic phenomenon in a channel scale, and a classical experiment can provide the data for verifying the result of CFD codes. The data however is not enough for validating the turbulence model used in the CFD code. The pressure loss in the complex configuration of commercial spacers arises from a several hydrodynamic effects included in the flow.

Thus the detailed data to validate the CFD becomes necessary. Various efforts were given to the simulations and measurements to obtain the flow field around the spacer. By applying commercial CFD codes to designing the spacer, availability of such turbulence models as the standard k-ε model (Oh, 2000, X.Z. Cui, 2003) and the nonlinear Speziale k-ε turbulence model (In, 2003) were recommended. Particle Imaging Velocimetry (PIV) technique provided flow structure in a sub-channel at immediately downstream of the grid spacer (McClusky, 2003), and Laser Doppler Velocimetry (LDV) provided streamwise component of higher order statistics (S.K. Yang, 1998). However, those simulation and experiment were not able to provide the data in the near wall region. The near wall data is important for assessing the turbulence model.

This study employs experimental and numerical works to validate a commercial code for predicting the pressure loss of a PWR grid spacer. The pressure loss for a full size spacer mock-up is measured to verify the numerical result of the commercial code, and a large eddy simulation (LES) for a typical PWR spacer configuration is performed to look at hydrodynamic effects on the pressure loss in the flow. In order to use the no-slip wall condition, the LES is performed at a low Reynolds number condition, and then the near wall phenomena can be observed better than at higher Reynolds number

condition. The FLUENT code (ANSYS FLUENT, 2007) is picked up as a commercial code, and the k-ε and RSM models with the universal law of the wall are used for turbulence model.

In Section 2, the experiment set-up and the result of the pressure loss measurement is explained. The LES with our original technique is performed and the flow field obtained is explained in Section 3. In Section 4, the commercial code is applied to the pressure loss prediction and is validated in comparison with the data obtained by the measurement and LES. The concluding remarks are placed in Section 5.

2. MESUREMENT OF PRESSURE LOSS

2.1 Experimental method

The test loop used for pressure drop measurement is shown in Fig.1. The pressure drop is measured for the flow at room temperature and pressure. The test loop is located at Kumatori Works in Nuclear Fuel Industries, Ltd.

The test loop is consists of a test section, a water storage tank, a volute pump and a cooling unit. The storage tank is open in the atmosphere, and it can maintain the flow steady without any mechanical control. The volute pump controls the flow rate, referring the indication of the electromagnetic flow meter. The cooling unit adjusts the temperature at the inlet of the test section.

Test section is inside a 216.5mm x 216.5mm square shroud with a mock-up of a PWR fuel assembly installed. The mock-up consists of 17 x 17 rods half an actual fuel rod. The diameter of the rod is 9.5 mm, and the pitch between the rods is 12.6mm. Pressure taps are located at upstream and downstream of spacer grid to measure the pressure loss of grid spacer and rod friction. The piezoelectric differential pressure transducer is used. Output of the transducer is transferred to data acquisition system within an accuracy of ± 0.001kgf/cm^2. Absolute pressure and fluid temperature are measured at the inlet of the test section.
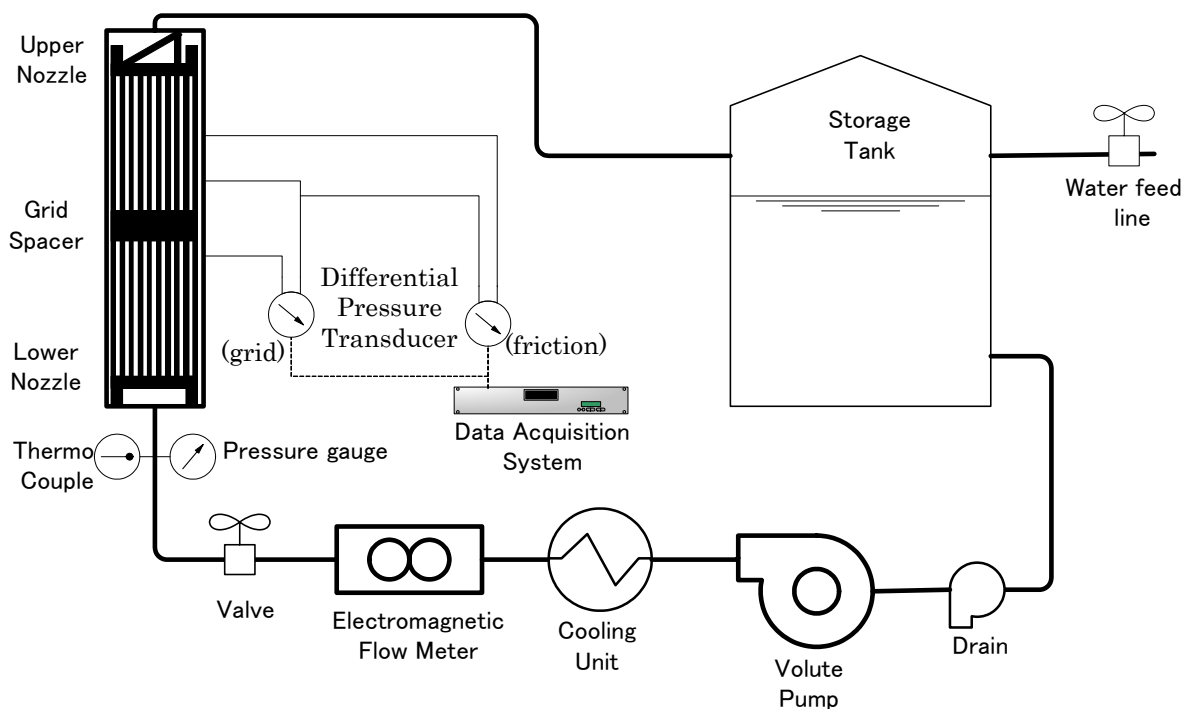

Figure 1. Experimental apparatus

Table 1. Outline of the test condition

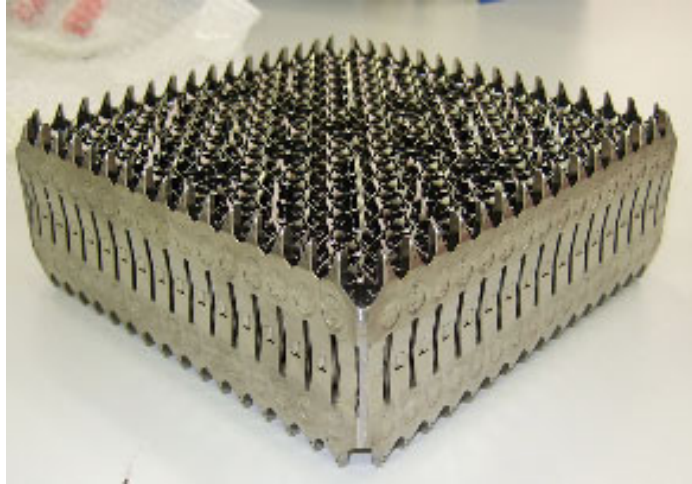| Pressure	Normal
Inlet temperature (Celsius degree)	40, 60
Flow rate (litre/min)	4000 – 9000
Reynolds number	40000 – 130000

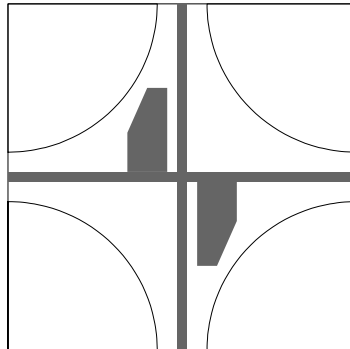Figure 2. Grid spacer with the standard inclination of mixing-vane

Figure 3. Split type mixing vane

Figure 4. Bending jig and angle gauge

Typical grid spacer used in this test is shown in Fig. 2. The height of spacer grid is approximately 60 mm. The mixing-vane type used is the split vane illustrated in Fig.3. The inclination angle of mixing-vane is the experimental parameter. The angle is adjusted with an accuracy of ±2 degree by using special tools (bending jig and angle gauge) shown in Fig. 4. The inclination of mixing vanes is decreased to -10 or increased to +10 degrees from a standard inclination. Outline of the test condition is summarized in Table 1.

2.2 Experimental result

The rod friction loss coefficients f is calculated as:

$$f = \frac{2D_H}{l\rho U_b^{\,2}}\Delta P_{f,l}, \tag{1}$$

where $\Delta P_{f,l}$ is the pressure difference between the taps at the distance l (approximately 200mm); D_H, ρ and U_b are respectively the hydraulic equivalent diameter, the fluid density and the bulk velocity. Next, the friction and drag loss coefficients are calculated as

$$K = \frac{2}{\rho U_b^{\,2}}\left(\Delta P_L - \Delta P_{f,L}\right) \tag{2}$$

where $\Delta P_{f,L}$ and ΔP_L are the pressure differences for the distance L (approximately 500mm); $\Delta P_{f,L}$ is calculated by using Eq.(1), and ΔP_L is measured between the taps located upstream and downstream of the spacer.
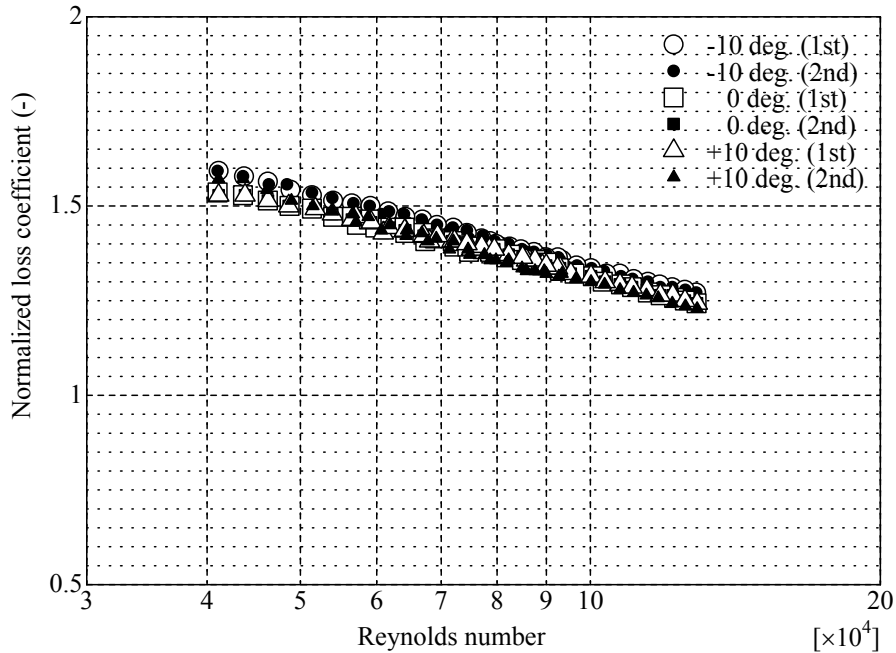

Figure 5. Pressure loss coefficient of friction of rod versus Reynolds number

The rod friction loss coefficient measured is shown in Fig. 5. The test is repeated twice for each inclination of mixing-vanes. As shown in Fig. 5, the data for the first and the second tests are similar enough to confirm the repeatability. The uncertainty appears approximately 10%. The data indicated that the rod friction loss is independent of the mixing-vane inclination and that the drag loss of the spacer is well separated from the friction loss. The drag loss coefficient obtained is processed into $K = A\,Re^{B}$ to evaluate its value at a higher Reynolds number condition. Here, Re is Reynolds number; the values of A and B are proprietary.

The drag coefficient at Re=420,000 is normalized by the value for the standard inclination and is shown in Fig. 6. The uncertainty is estimated at 10%. The dependency on the vane inclination is not linear but parabolic, and the result can be expressed by $K = a\,sin^{2}\,\theta + b$, where θ is a vane inclination; the values of a and b are proprietary. This formulation is derived based on a precedent study (Rehme, 1973), where the loss coefficient was proportional to ε^{2}. Here, ε is the relative plugging of the flow section; the plugging accounts for the cross-sectional projection of the spacer configuration. If only the cross-sectional projection of the mixing-vane is taken into account, the effect of θ on the loss coefficient is represented by $sin^{2}\,\theta$.

The experimental result however shows a change faster than $sin^{2}\,\theta$. The thickness of the soft and hard stops of spacer grid may cause more complex change in the projected area. The plugging ε is calculated for the actual geometry, and the formula $K = c\,\varepsilon^{2} + d$ is obtained. Here, the values of c and d are proprietary. Figure 6 shows that the latter represents better than the former.
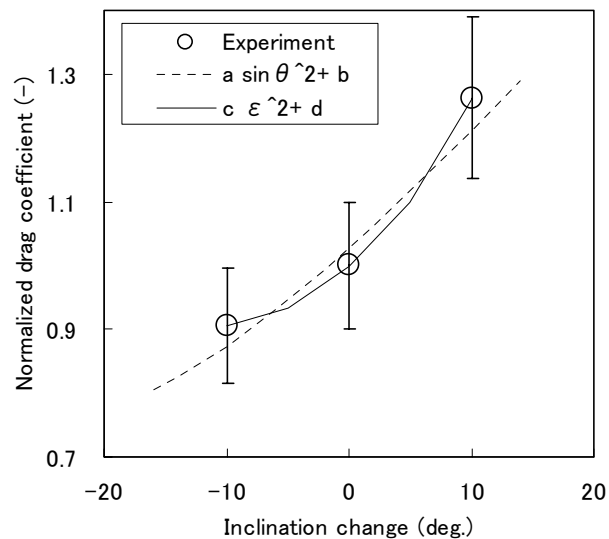

Figure 6. Experimental result for drag coefficient

3. MECHANISM OF PRESSURE LOSS

3.1 LES of the turbulent flow

LES is performed to understand the flow around the PWR spacer grid and to validate the turbulence model used in the commercial CFD code. The LES code was developed by using our original technique of the immersed boundary method (Ikeno, 2007a). This code represents complicate wall configuration on the Cartesian grid system, and this can achieve the second-order spatial accuracy of the discrete equation. The outline of the numerical method is described in this section.

The continuity and Navier-Stokes equations for incompressible flow are used for mass and momentum conservation laws. Applying the filtering operation to them and assuming an eddy viscosity model for sub-grid scale (SGS) stress results in the governing equations for LES.

$$\frac{\partial u_i}{\partial x_i} = 0, \ (i = 1, 2, 3)$$ (3)

$$\frac{\partial u_i}{\partial t} + u_j \frac{\partial u_i}{\partial x_j} = -\frac{\partial p}{\partial x_i} + \frac{\partial}{\partial x_j}\left[\left(\nu + \nu_{SGS}\right)\left(\frac{\partial u_i}{\partial x_j} + \frac{\partial u_j}{\partial x_i}\right)\right] + \frac{4\delta_{i1}u_T^2}{D_H},$$ (4)

where

x_i : the i-th coordinate distance in Cartesian system,

u_i : the i-th component of filtered velocity,

p : filtered pressure deviation from the mean value divided by the fluid density,

u_T : average friction velocity,

D_H : hydraulic equivalent diameter,

$\delta_{i,1}$: Kronecker delta,

ν : kinematic viscosity for molecular viscous stress,

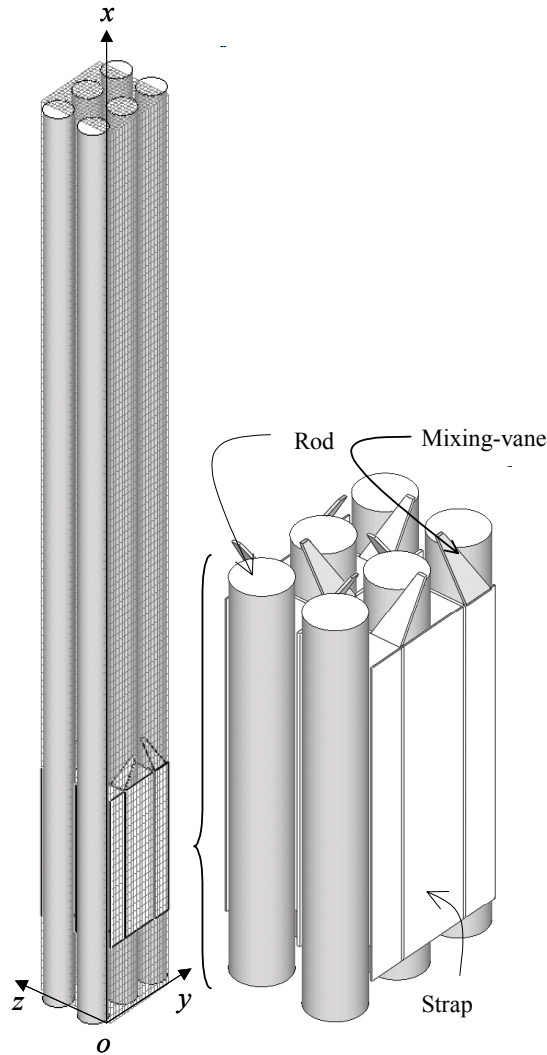ν_{SGS} : kinematic viscosity for SGS viscous stress.

Figure 7. Computational domain and spacer configuration

The third term in the right-hand side of Eq.(4) represents the mean pressure gradient to drive the mainstream constantly. The SGS viscosity is determined by using the solution of the one-equation dynamic SGS model (Kajishima, 2006).

The discrete equations for Eqs.(3) and (4) are based on the second-order central finite differential method. The no-slip wall condition in the LES is simulated on Cartesian grid system by using our original immersed boundary method (Ikeno, 2007a). In this method, the time integration is carried out using a numerical scheme that was developed for unsteady turbulence simulations to achieve the no-slip wall condition precisely.
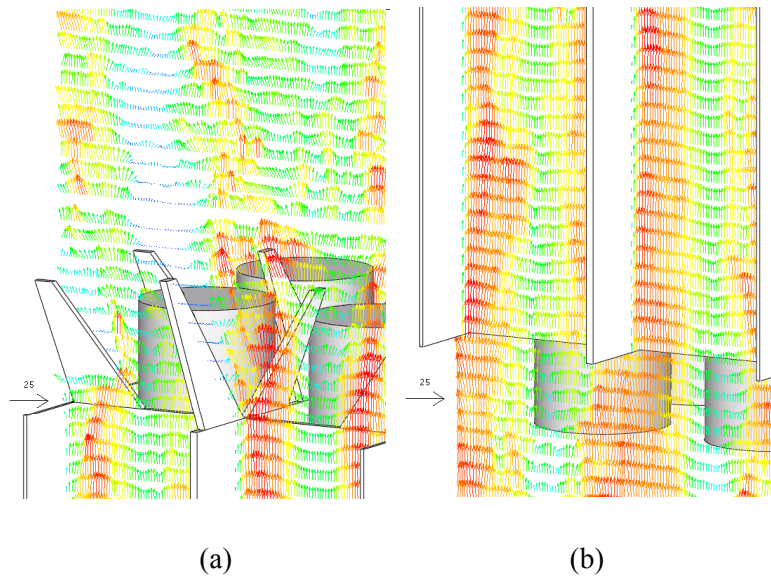

(a)   (b)

Figure 8. Instantaneous flow around (a) the mixing-vanes, (b) the bottom of the strap

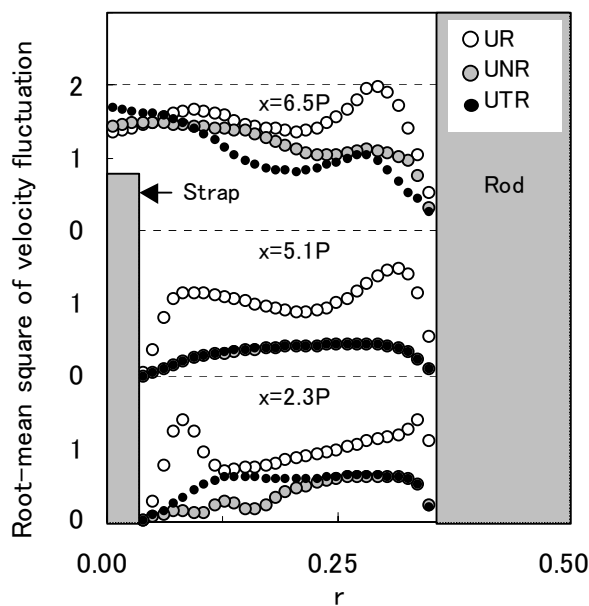Figure 9. Velocity fluctuations in the spacer
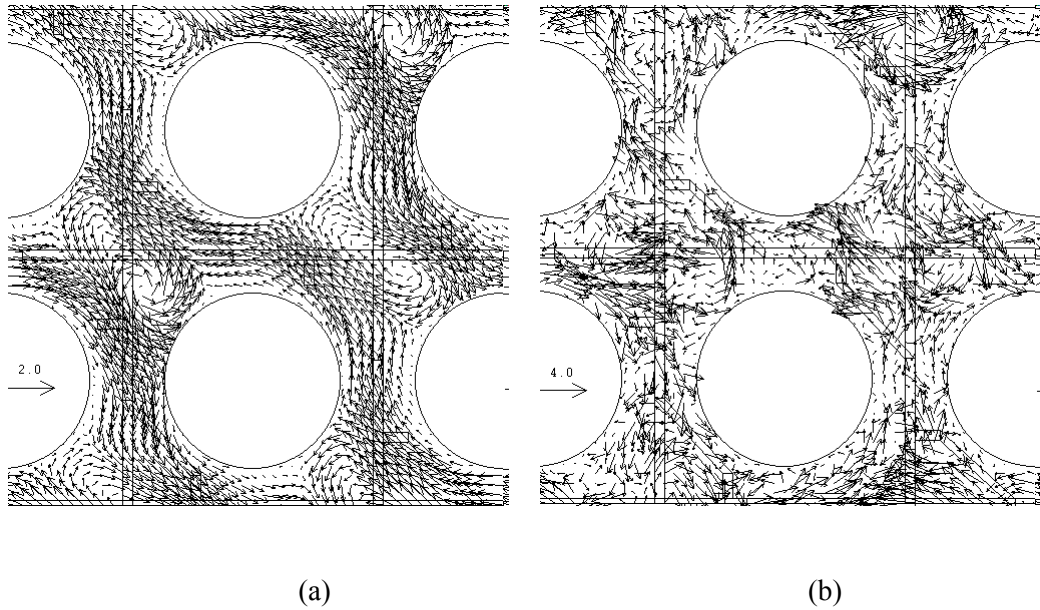
<div align="center">(a)   (b)</div>

Figure 10. Lateral flow pattern (a) averaged flow, (b) instantaneous flow.

The computational domain with the computational grid system and the configuration for the grid spacer are shown in Fig. 7. The computational domain is composed of 4 sub-channels. The number of grid points used in the computation is *512* x *256* x *256* in each direction of *x*, *y* and *z*. The main flow is in the direction of positive *x*. The no-slip condition for a static object is given by the immersed boundary method (Ikeno, 2007a), forcing zero velocity on the surface and inside the body to fuel rods and the grid spacer. The periodic boundary condition is applied to all the boundaries of this computational domain to simulate a whole rod assembly. The configuration of the grid spacer is simplified from that of the actual one by omitting complicate structures (Ikeno, 2006).

The Reynolds number achieved in the LES is approximately *4100*, which is too low to compare with our pressure loss experiment. Here, the Reynolds number is based on bulk velocity and rod pitch. The drag coefficient obtained is therefore compared with data in the existing literatures, and the convergence to the experiment as the mesh resolution become fine was confirmed (Ikeno, 2006).

3.2 Mechanism of the flow

After the flow reached fully developed state, we pick up an instantaneous velocity field around the spacer as shown in Fig.8. Figure 8(a) indicates a large-scale unsteadiness behind the mixing-vane, which relates to the acceleration of the swirling flow (Ikeno, 2005b). Figure 8(b) indicates that the mainstream is divided by the strap at the subchannel center, where the turbulence differs from the turbulence developed near the plane wall. In those phenomena, the turbulent energy in the mainstream is transferred insufficiently into the lateral direction and then the standard k-ε model is not applicable.

To characterize the turbulence around the spacer, the root-mean square of velocity fluctuation is shown in Fig.9. The statistical data is obtained by averaging the flow fields during the time integration in the region with spatial symmetry. The result for *x=2.3P* shows that the streamwise components are dominant near the strap. This is because the shear turbulent stress is undeveloped at the beginning of no-slip wall. This trend becomes moderated as the turbulence develops along the strap (see, *x=5.1P*). At *x=6.5P*, the turbulence is active to retrieve the velocity profile in the wake region behind the strap. The turbulent flow around the spacer is thus undeveloped statistically.

Main factor causing the pressure loss of the spacer is the drag loss. It arises from the plugging of the flow area by the projection of the mixing-vane area and strap thickness. The flow separated above the mixing-vanes and the wake behind the strap will affect the drag loss of the spacer. Another factor to cause the pressure loss is the friction loss along the faces of rods and the straps. Averaged and instantaneous flows in the cross-sectional flow are shown in Fig. 10. Figure 10(b) shows a complex pattern of the instantaneous flow. The turbulence stress arises from its deviation from the averaged flow, and the result implies complicate contribution of the turbulent stress to the friction loss.

4. PREDICTION OF PRESSURE LOSS

4.1 Numerical method

For predicting pressure loss of spacer, the commercial code FLUENT is picked up as a commercial CFD code. The FLUENT code solves conservation law of mass and momentum with widely used constitutive equation, namely the turbulence model or near wall treatment (ANSYS FLUENT, 2007). The finite volume method is employed as discretization.

The computational domain covers 2 by 2 spacer cells horizontally and a spacer interval axially. Rod diameter, rod spacing and the shape of spacer simulate those used in the pressure loss test. To reduce the computational cost, a slab model equipped in the FLUENT code is applied to the grid strap and mixing-vanes. This model can represent the impermeability and the no-slip on the wall without using mesh in the thickness. For reference of computational geometry, the surface mesh on the spacer is illustrated in Fig. 11.
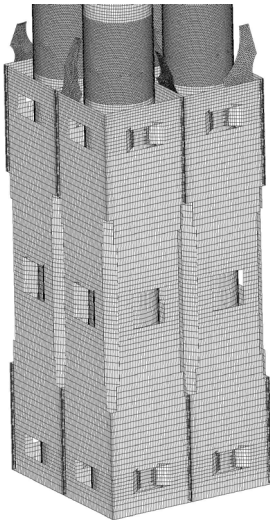

Figure 11. Mesh on the spacer surface

Table 2. Turbulence model

Turbulence stress model	Wall function model
Two-equation k-ε model (KE)	Standard (STD)
Two-equation k-ε model (KE)	Non-equilibrium (NEQ)
Reynolds stress model (RSM)	Non-equilibrium (NEQ)

Pressure and velocity are solved sequentially by SIMPLE method. From the discretization scheme option, "the second order upwind scheme" and "the second order central scheme" are chosen for the convection and diffusion terms, respectively. The periodic condition is applied to the computational domain to maintain a constant mass flow rate in the axial direction. The Reynolds number is approximately 400,000 and is high enough for Reynolds averaged method to be applied. The k-ε model and the Reynolds stress model are therefore used together with near-wall models: FLUENT standard wall functions and non-equilibrium wall function. The combinations used for turbulence stress and wall function models are shown in Table 2. The NEQ is a wall function that can represent a velocity distortion caused by an inversed pressure gradient, and RSM is capable to represent more complex flow including separation and wake.
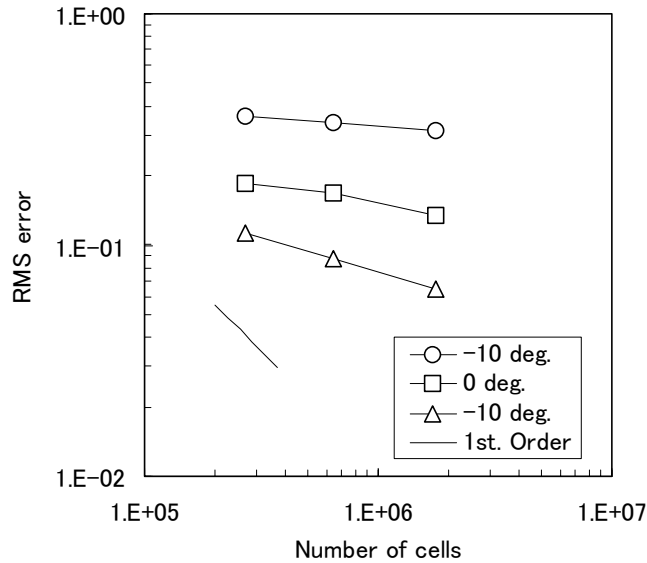

Figure 12. Accuracy of predicted drag coefficient

4.2 Numerical result

The average pressure loss obtained by the FLUENT code is used to calculate the pressure loss coefficient. The drag loss is evaluated by subtracting the friction loss from the total loss. Here, predicting the friction loss is difficult for the numerical simulation using the wall functions, and the friction coefficient is estimated by an empirical equation. The drag coefficient of spacer is calculated by using the mean bulk velocity consistent with the flow rate given in the boundary condition.

To check the mesh refinement, the number of computational grid is increased up to 640,000 and 1770,000. Root mean square of the error between the prediction and the experiment is shown in Fig. 12. The figure shows that the accuracy of the prediction is less than the first-order whereas the discretization option advocates "the second order". It is noted that the numerical accuracy strongly depends on the mesh geometry. The result indicates that the error is hardly improved by the fine mesh. This implies that the grid number of 270,000 is enough to obtain the converged solution for this discrete equation system.

Figure 13 shows comparison between predicted and measured values for drag coefficient as a function of mixing vane inclination. The computation is performed using 270,000 grids. The value is normalized by that measured for the standard inclination. The computational prediction goes below the

experiment as the inclination becomes small. This indicates that the prediction approaches the drag coefficient of spacer with zero thickness whereas the experiment does that with a finite thickness.

Generally, the prediction reproduces the trend of the drag coefficient independently of the turbulence model. This suggests that a large-scale unsteadiness and an undeveloped turbulent flow around the spacer are not dominant for predicting the drag loss.
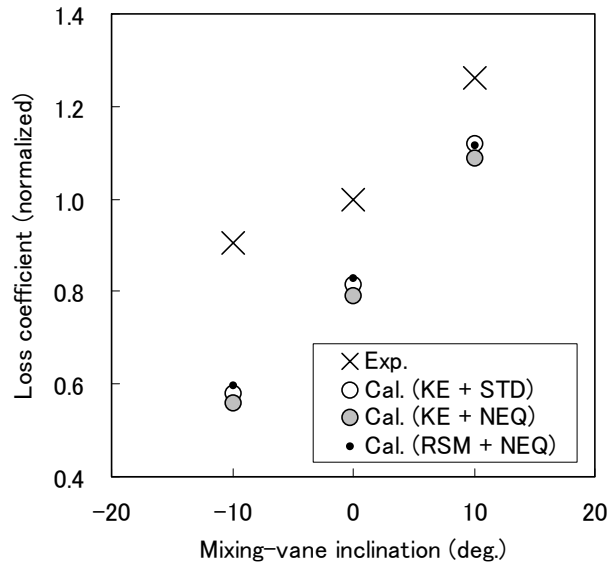

Figure 13. Numerical result for drag coefficient

5. CONCLUSION

A pressure loss measurement and an LES were performed to validate a commercial CFD code for predicting the pressure loss of a PWR grid spacer. The experimental data was obtained for full size spacer mock-ups with three steps of the inclination angle of the mixing-vane, and the LES was performed with *512* x *256* x *256* grids.

The experimental data of pressure loss is macroscopic, and it was thought to be useless for validating directly the turbulence model used in the CFD code. The LES was therefore used to clarify the physics in the flow around the spacer. The result indicated that the flow field around the spacer included a large-scale unsteadiness and an undeveloped turbulent flow. Moreover, it suggested that the friction loss was affected by complicated turbulence and that predicting the friction loss was difficult.

The commercial code with the standard high Reynolds number k-ε model with the law of the wall however successfully reproduced the trend of the measurement. This suggests that a large-scale unsteadiness and an undeveloped turbulent flow are not dominant for the drag loss. It is noted that commercial codes should be applied to the flows where dominant physics is clarified.

REFERENCES

ANSYS FLUENT Inc., 2007, Fluent 6.3 User's Guide

W.K. In, D.S. Oh, T.H. Chun, "Simulation of turbulent flow in rod bundles using eddy viscosity models and the Reynolds stress model", *Proceedings of international topical meeting on Nuclear Reactor Thermal Hydraulics (NURETH10)*, 48, CD-ROM E00213 (2003).

K. Rehme, "Pressure drop correlations for fuel element spacers", *Nuclear Technology*, Vol.17, pp.15-23 (1973).

D.S. Oh, W.K. In, T.H. Chun, "Structure of turbulent flow in sub-channel of rod bundle downstream of spacer grid with flow mixing device", *Procceding of the 4th JSME-KSME Thermal Engineering Conference*, B215 (2000).

H.L. McClusky, M.V. Holloway, T.A> Conover, D.E. Beasley, "Mapping of the lateral flow field in typical subchannels of a support grid with vanes", *J.Fluids Engineering*, Vol.125, pp.987-996 (2003).

S. K. Yang and M. K. Chung, "Turbulent Flow Through Spacer Grids in Rod Bundles", *Journal of Fluids Engineering*, Vol.120, No.4, pp.786-791 (1998).

T. Ikeno and T. Kajishima, "Decay of Swirling Turbulent Flow in Rod-bundle", *Journal of Fluid Science and Technology*, Vol.1-1, pp.36-47 (2006).

T. Ikeno and T. Kajishima, "Finite-difference immersed boundary method consistent with wall conditions for incompressible turbulent flow simulations", *Journal of Computational Physics*, Vol.226-2, pp.1485-1508 (2007a).

T. Ikeno and T. Kajishima, "Computational Model for Turbulent Flow Around a Grid Spacer with Mixing Vane", *Nuclear Technology*, Vol.158, pp.249-260 (2007b).

T. Kajishima and T. Nomachi, "One-Equation Subgrid Scale Model Using Dynamic Procedure for the Energy Production", *ASME J. Appl. Mech.*, Vol.73-3, pp.368-373 (2006).

X.Z. Cui and K.Y. Kim, "Three-dimensional analysis of turbulent heat transfer and flow through mixing vane in a subchannel of nuclear reactor", *Journal of Nuclear Science and Technology*, Vol. 40, No. 10, pp.719-724 (2003).